

5.6 NUMERICAL MODELS OF ENTRAINMENT INTO SHEARED CONVECTIVE BOUNDARY LAYERS EVALUATED THROUGH LARGE EDDY SIMULATIONS

Robert Conzemius* and Evgeni Fedorovich
 School of Meteorology, University of Oklahoma, Norman, Oklahoma

1. INTRODUCTION

Atmospheric convective boundary layer (CBL) entrainment is the downward mixing of free atmospheric air into the CBL as the CBL grows. Primarily, the CBL entrainment is driven by the buoyancy production of turbulence kinetic energy (TKE) due to heating of the lower surface or cooling at the CBL top. The effects of shear-generated turbulence in the CBL are secondary. However, cases of a purely buoyancy-driven CBL are rare, and in many situations, the flux of buoyancy is relatively weak, allowing the effects of shear-generated turbulence to become roughly equivalent to those of buoyancy-generated turbulence

Large eddy simulation (LES), which can resolve most of the energy-containing motions in the CBL, has become a standard tool for fundamental studies of the CBL dynamics. However, the spatial and temporal resolution needed in the LES for an adequate reproduction of the CBL turbulence properties is still beyond the limits of numerical models commonly employed for weather prediction purposes, as well as in applied climate and air pollution research. In the present study, we use LES to evaluate predictions of entrainment into the sheared CBL by numerical models of two types: (i) models with turbulence closure schemes based on Reynolds averaging, which resolve some vertical structure of the CBL and are commonly applied in numerical weather prediction (NWP) and (ii) models based on vertically integrated momentum, buoyancy, and TKE balance equations assuming a parameterized CBL vertical structure (the integral budget approach). The latter approach is widely used to predict integral CBL parameters (e.g., depth of convectively mixed layer) in applied atmospheric dispersion studies.

Previously, Moeng and Wyngaard (1989) have evaluated NWP turbulence closures for parameterizing the turbulence structure of shear-free CBLs, and Ayotte et al. (1996) have done the same for both sheared and shear-free CBLs.

2. REYNOLDS AVERAGING-BASED TURBULENCE CLOSURE SCHEMES

Two turbulence closure schemes, based upon

Reynolds averaging (RANS), such as used in NWP, are evaluated here. The two schemes are both 1.5 order, $e-l$ closure schemes and therefore, both have the same basic formulations of the TKE equation, eddy diffusivities of heat and momentum, and dissipation. The differences between these two schemes are in the specification of the length scale used to close the problem and in constants in the expressions for the eddy diffusivities and TKE dissipation.

In the actual NWP grids used at the time of this writing, the grid cell size is becoming small enough that the implied horizontal averaging of the non-resolved turbulence within the grid cell may differ considerably from an ensemble average. As such, the assumptions used in the RANS-based NWP turbulence closures may not hold. This is a particularly important problem in contemporary NWP. However, in this evaluation, it is assumed that the grid cell sizes are large enough that the implied horizontal averaging *can* be considered representative of an ensemble average, and the assumptions of a Reynolds averaging-based scheme will still be valid.

In such a case, the TKE equation has the following form:

$$\frac{\partial \langle e \rangle}{\partial t} = -\langle wu \rangle \frac{\partial \langle U \rangle}{\partial x} - \langle wv \rangle \frac{\partial \langle V \rangle}{\partial x} + \frac{g}{\theta_0} \langle w\theta' \rangle - \frac{\partial}{\partial z} \left(\langle we \rangle - \frac{1}{\rho_0} \langle wp' \rangle \right) - \varepsilon, \quad (1)$$

where e is the TKE, U and V are the total horizontal components of the flow, u , v , and w are the turbulent components, p' and θ' are the deviations of pressure and potential temperature from their horizontal averages, g is the acceleration of gravity, θ_0 is the reference value of potential temperature, ε is dissipation of TKE, and brackets denote averaged quantities.

The turbulent fluxes are parameterized according to the following hypotheses:

$$\langle we \rangle + \frac{1}{\rho_0} \langle wp' \rangle = -2K_m \frac{\partial \langle e \rangle}{\partial z}, \quad (2)$$

$$\langle wu \rangle = -K_m \frac{\partial \langle U \rangle}{\partial z}, \quad (3)$$

$$\langle wv \rangle = -K_m \frac{\partial \langle V \rangle}{\partial z}, \text{ and} \quad (4)$$

* *Corresponding author address:* Robert J Conzemius,
 School of Meteorology, University of Oklahoma, 100 East
 Boyd, Norman, OK 73019-1013;
 e-mail: bconzemi@rossby.metr.ou.edu

$$\langle w\theta' \rangle = -K_h \frac{\partial \langle \theta \rangle}{\partial z}, \quad (5)$$

where K_m and K_h are the eddy diffusivities of momentum and heat, respectively. The eddy diffusivity of momentum has the following general form:

$$K_m = \alpha_K e^{1/2} l \quad (6)$$

where α_K is a constant, and l is a turbulence length scale. The eddy diffusivity for heat is related to the eddy diffusivity for momentum through the turbulent Prandtl number, which generally ranges from one third to one under unstable conditions. Dissipation is parameterized by the expression

$$\varepsilon = \alpha_\varepsilon \frac{e^{3/2}}{l}, \quad (7)$$

where α_ε is a constant. The values of α_K , α_ε , l , and the turbulent Prandtl number are scheme-dependent.

The first scheme evaluated in this study is that of Xue et al. (2001). The turbulence length scale in this closure is dependent on the hydrostatic stability. In stable conditions, the length scale is

$$l_s = 0.76 \langle e \rangle^{1/2} N^{-1}, \quad (8)$$

where N is the Brunt-Väisälä frequency. In neutral or unstable conditions (the boundary layer portion of the flow), the length scale is

$$l_u = l_0 \left\{ 1.8z_i \left[\begin{array}{l} 1 - \exp(-4z/z_i) \\ -0.0003 \exp(8z/z_i) \end{array} \right] \right\} \quad (9)$$

where z is the height, z_i is the boundary layer depth, and $l_0 = 0.25$. The boundary layer depth is defined as the level at which a parcel, lifted from the lowest model grid level above ground, becomes neutrally buoyant. Because l_u doesn't become small until $z > z_i$, where the atmosphere is stable, the maximum of l_s and l_u is taken. The turbulent Prandtl number is

$$\text{Pr}_t = \max \left[\frac{1}{3}, \left(1 + \frac{2l}{\Delta_v} \right)^{-1} \right], \quad (10)$$

where Δ_v is the vertical dimension of grid cell. The constants in (6) and (7) are $\alpha_K = 0.1$ and $\alpha_\varepsilon = 3.9$ at the first grid level above ground and $\alpha_\varepsilon = 0.93$ at all other grid points.

The scheme of Fiedler and Kong (2003), hereafter referred to as F&K, does not depend on the determination of the CBL depth. Rather, it defines the

length scale as the geometric mean of an upward length scale and a downward length scale. The upward and downward length scales are defined as the vertical distance an air parcel would travel from its original height, working against buoyancy forces, until all its TKE were expended. Mathematically, these length scales are defined through the following integrals:

$$e(z) = \int_z^{z+\lambda_{up}(z)} \frac{g}{\theta_v(z')} \left[\overline{\theta}_v(z') - \overline{\theta}_v^*(z, z') \right] dz', \quad \text{and} \quad (11)$$

$$e(z) = \int_z^{z-\lambda_{down}(z)} \frac{g}{\theta_v(z')} \left[\overline{\theta}_v(z') - \overline{\theta}_v^*(z, z') \right] dz', \quad (12)$$

where λ_{up} and λ_{down} are the vertical distances of parcel travel and θ_v^* is the virtual potential temperature a parcel would have if it ascended or descended from its starting level z to a new level z' . Once λ_{up} and λ_{down} are determined, the mixing length is $l = (\lambda_{up}\lambda_{down})^{1/2}$. The specifications for the constants are $\alpha_K = 0.25\sqrt{2} = 0.35$, $\alpha_\varepsilon = 0.5$, and $\text{Pr}_t = 1$.

3. CLOSURE SCHEMES BASED ON INTEGRAL BUDGETS

To simplify the numerical complexity and computational cost and to develop a conceptual understanding of CBL growth, the horizontally averaged profiles of buoyancy, momentum, and TKE (Eq. 13) can be integrated over the depth of the CBL to form the integral budgets of those quantities. In order to simplify the integration, the boundary layer structure is parameterized. The simplest parameterization is known as the zero order model (ZOM), developed by Lilly (1968) and others following. Figure 1 shows the ZOM profiles for buoyancy. In the ZOM, the buoyancy is taken to be constant within the CBL and has a finite discontinuity at the CBL top, where it jumps to its free atmospheric value. Above the CBL, the buoyancy is a linear function of height. Integrating the buoyancy balance equation to some arbitrary level $z < z_i$, one can obtain the buoyancy flux, which varies linearly from a positive value at the surface to a negative value just below the interface at the CBL top (a fraction of the negative of the surface value), where it jumps back to zero. Originally, the ZOM was only applied to situations in which the shear contribution of TKE in the CBL could be neglected, but later authors [Zeman and Tennekes (1977), Tennekes and Driedonks (1981), Driedonks (1982), Boers et al. (1984), Fairall (1984), Batchvarova and Gryning (1990, 1994), Fedorovich (1995), Pino et al. (2003) extended it to CBL types with shear contribution to the generation of TKE. The momentum profiles in the ZOM are prescribed in a similar manner to the buoyancy profile, with a constant value in the mixed layer, a jump at the top of the CBL, and a linear rate of change in the free atmosphere. Fedorovich (1995)

derived the complete ZOM equations for the CBL with wind shear contributions to the TKE but did not propose solutions to the equations.

For the shear-free case, analytic solutions to the entrainment equation are possible when certain assumptions are made regarding the profiles of TKE and its dissipation rate. In particular, the Deardorff (1970) and Zilitinkevich and Deardorff (1974) scaling hypotheses are used, and the TKE and dissipation profiles in the CBL are assumed to be self-similar. Given such assumptions, the TKE and dissipation, when scaled by the convective velocity scale $w_* = (B_s z_i)^{1/3}$, integrate to constants, and the system of equations describing CBL entrainment is closed. Fedorovich et al. (2004) have compared ZOM solutions with LES of the shear-free CBL and found good agreement as long as the parameters of entrainment are retrieved from LES in a manner that is consistent with their definitions in the ZOM.

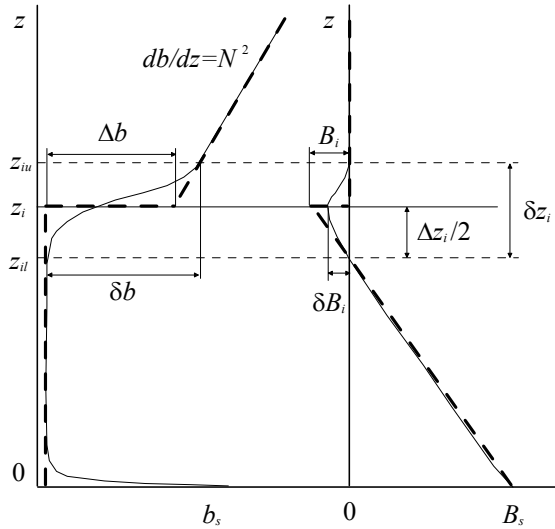


Figure 1. Profiles of buoyancy in the zero order model (ZOM) compared to the actual horizontally averaged profiles in the CBL.

Similar scaling assumptions regarding the integrals of TKE and dissipation can be applied to the CBL with shear, except that the appropriate velocity scale may be different from the shear-free case. In the ZOM, the shear generation of TKE within the CBL is zero because the momentum is assumed to be well-mixed there. This means that shear only contributes to the generation of TKE at the CBL top or at the surface. Most authors consider the surface shear and adjust the velocity scale upward by including the friction velocity u_* .

At the CBL top, the shear contribution is modeled in terms of the velocity jumps, and the assumption is made that a certain fraction of the shear-generated energy is available for entrainment, and the other portion is dissipated.

The derivations of the entrainment equations are found in the papers listed above, and the equations are only listed in their final form here. Some authors present their solutions in terms of the CBL growth rate, dz_i/dt , and others show the entrainment flux ratio, which is defined as the negative of the buoyancy flux of entrainment to the surface buoyancy flux ($-B_i/B_s$). In terms of the latter quantity, the following general form is common to most of the equations:

$$-\frac{B_i}{B_s} = \frac{\Delta b}{B_s} \frac{dz_i}{dt} = \frac{w_m^3}{w_*^3} \left[\frac{C_F}{1 + C_T \frac{w_*^2}{\Delta b z_i} - C_P \frac{(\Delta u^2 + \Delta v^2)}{\Delta b z_i}} \right] \quad (13)$$

where Δu and Δv are velocity jumps across the entrainment zone and Δb is the buoyancy jump. $B_i = (g/\theta_0)\langle w\theta' \rangle_i$ ($= -\Delta b dz_i/dt$ in the ZOM) is the buoyancy flux of entrainment, $w_* = (B_s z_i)^{1/3}$ is the Deardorff (1970) convective velocity scale and C_F , C_T , and C_P are constants describing the relative contributions of the buoyancy generation, spin-up, and shear generation of TKE, respectively. The parameter C_F represents the portion of buoyancy-generated TKE that is not dissipated before being used for entrainment, and C_P represents the portion of shear-generated TKE that is available for entrainment. Finally, the adjusted velocity scale is $w_m^3 = w_*^3 + Au_*^3$, where u_* is the friction velocity, except Zeman and Tennekes (1977) and Tennekes and Driedonks (1981) use $w_m^2 = w_*^2 + Au_*^2$.

One limitation of (13) is immediately clear: if the shear across the CBL top becomes sufficiently large, the denominator of the entrainment equation can go to zero, and the entrainment ratio will become infinite. While this result is expected if the surface buoyancy flux approaches zero, it is not clear from the expression that the right hand side will behave in such a fashion. Some of this has to do with the limitations of the assumptions that are made, particularly with the spin-up term. The spin-up of TKE is scaled only by the convective velocity scale, implying that the shear-generated TKE at the CBL top is not transported into the CBL where it is stored. If the shear is included in the velocity scale, then the spin-up term in the denominator will become larger and compensate for a larger shear term.

The entrainment parameterizations of Zeman and Tennekes (1977), Tennekes and Driedonks (1981), Boers et al. (1984), and Pino et al. (2003) follow (13) reasonably closely, except that Zeman and Tennekes (1977) were unable to include the entrainment zone shear term because they did not know what portion of the shear-generated TKE is available for entrainment. Table 1 describes the values of the constants that were used in the entrainment expressions.

Table 1. Values of Constants in Entrainment Equations

Author	A	C_F	C_T	C_P
Tennekes (1973)	12.5	0.2	0	0
Zeman and Tennekes (1977)	4.6*	$0.5 - 0.024 \frac{Nz_i}{w_m}$	3.55	0
Tennekes and Driedonks (1981)	4*	$0.6 - 0.03 \frac{Nz_i}{w_m}$	4.3	0.7
Driedonks (1982)	25	0.2	0	0
Boers (1984)	23	0.32	0.75	1
Batchvarova and Gryning (1990,1994)	12.5	0.2	0	0
Pino et al. (2003)	8	0.2	4	0.7

Other studies [Tennekes (1973), Driedonks (1982), Batchvarova and Gryning (1990,1994)] consider only the surface shear or parameterize the total shear contribution. In this case, (13) is reduced to $-B_i/B_s = w_m^3/w_s^3$. Batchvarova and Gryning (1990, 1994) use the formula

$$-\frac{B_i}{B_s} = \frac{X(1+X)}{1+X+Y(1+2X)} \quad (14)$$

where $X = w_m^3/w_s^3 = C_F(1+Au^3/w_s^3)$ and $Y = Bu^2/N^2z_i^2$, with $B = 8$.

The entrainment equation of Stull (1976a,b) partially follows the ZOM approach but adds a parameterization of the entrainment zone thickness over which the velocity jump occurs. Although his approach is somewhat inconsistent with ZOM methodology, the problems of the unboundedness of (13) are avoided. Stull's entrainment equation is

$$-\frac{B_i}{B_s} = A_1 + A_2 \frac{z_i}{\delta} \frac{u_m^2}{w_s^3} + A_3 \frac{z_i}{\delta} \frac{\Delta u^3}{w_s^3}, \quad (15)$$

where δ is the entrainment zone thickness, u_m is the mixed layer velocity, and $A_1 = 0.1$, $A_2 = 0.05$, and $A_3 = 0.001$.

More recently, Sorbjan (2004) developed a parameterization specifically for the heat flux at the sheared CBL top. This parameterization takes into account the Richardson number of the entrainment zone and therefore requires a finite entrainment zone thickness. In the ZOM, the entrainment zone Richardson number is zero because the entrainment zone depth is infinitesimally small while the velocity jump remains finite. Thus, shear becomes infinitely large and although the buoyancy gradient is also large, if one assumes a linear variation of buoyancy and

momentum across the entrainment zone and takes the limit as the entrainment zone depth goes to zero, one will find that the Richardson number tends to zero. The Sorbjan parameterization is

$$B_i = c_H w_s^2 N_i \frac{(1+c_2/Ri)}{(1+1/Ri)^{1/2}} \quad (16)$$

with $c_H = 0.015$ and $c_2 = 1.5$. The Richardson number is the interfacial Richardson number $Ri = \Delta b \delta / (\Delta u^2 + \Delta v^2)$, where the velocity and buoyancy jumps are interpreted as their changes across the full layer δ . This approach is most consistent with the first order model (FOM) of entrainment (Betts 1974), in which the buoyancy profile is like the ZOM profile in the mixed layer and the free atmosphere, but the entrainment zone has a finite thickness δ , and the buoyancy and velocity profiles there are linear.

Other FOM models [Mahrt and Lenschow (1976), Kim (2001)] have been considered for this study, but the mathematical formulation of the entrainment equation is not much different from (13) other than being a bit more complex. Additionally, the entrainment zone thickness is an additional dependent variable in the FOM equations that requires additional parameterizations or assumptions to close the problem and presents more opportunities for the developed equations to have undesirable mathematical consequences. Fairall (1984) also developed a shear parameterization for CBL entrainment, but the expression was rather cumbersome to evaluate from LES data and did not provide additional insight beyond what was provided by the simpler, ZOM-based entrainment equations.

4. EVALUATION METHODOLOGY

The following cases of CBL with wind shears were studied with LES:

1. No mean shear (**NS** case), which was the reference case.
2. Height-constant geostrophic wind of the 20 m/s magnitude throughout the whole simulation domain (**GC** case).
3. Geostrophic wind with the magnitude that linearly increased from zero at the surface to 20 m/s at the domain top (**GS** case).

In the **GC** and **GS** cases, geostrophic wind had only the longitudinal (x) component u_g , so the y component of the geostrophic wind, v_g , was set equal to zero. For all simulated cases, the surface roughness length, geographic latitude, and reference temperature were prescribed to be 0.01 m, 40° N, and 300 K, respectively.

In the initial-flow configurations (see Fig. 2), virtual potential temperature θ changed vertically at a constant rate of 0.001, 0.003, or 0.010 K/m throughout the entire domain starting from the surface. The initial wind velocity in the domain was geostrophic (zero in the **NS** case), with the vertical velocity component set equal to zero. The surface heat flux had values of 0.03, 0.10, or

0.30 K m/s and was kept constant with time throughout the run.

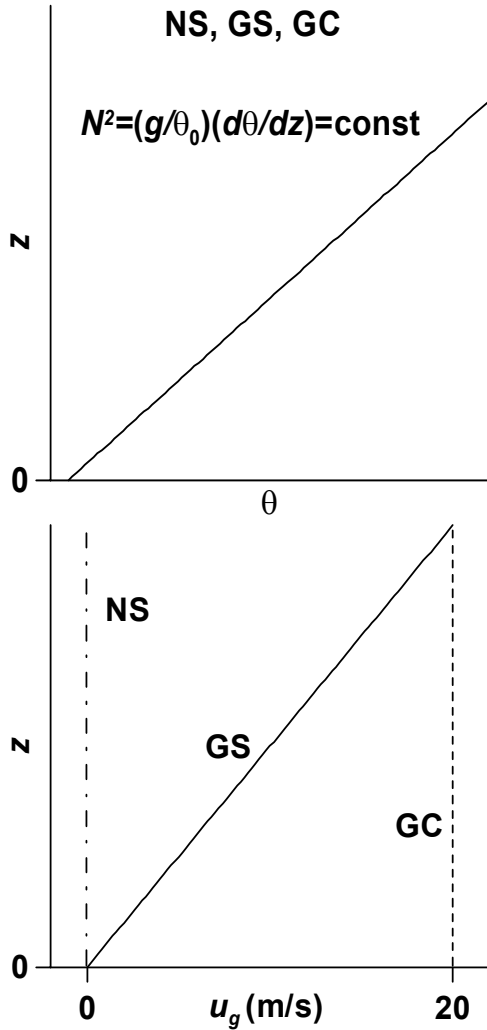


Figure 2. Initial profiles of the virtual potential temperature θ and x component of the geostrophic wind velocity, u_g , for the simulated CBL cases.

The LES grid domain was $5.12 \times 5.12 \times 1.6$ km with grid cells of 20 meters in all dimensions. Considering all possible combinations of shear, stratification, and surface heat flux, a total of 24 LES runs were conducted. The combinations with the strongest stratification (0.010 K/m) and weakest heat flux (0.03 K/s) were not conducted due to the excessive time necessary for these cases to run to completion. The LES were allowed to continue until the CBL depth reached approximately 1000 meters, at which point it was possible for the entrainment zone to impinge upon the sponge layer, so the run was stopped.

Turbulence statistics were calculated every 100 seconds. The averaging was carried out over the horizontal planes only in order to avoid uncertainties associated with complementary time averaging. The

CBL depth z_i was determined from the minimum of kinematic heat flux $\langle w\theta' \rangle$ (resolved + subgrid).

The evaluation of the RANS-based NWP turbulence closures was carried out in a similar manner to Moeng and Wyngaard (1989) and Ayotte et al. (1996). The LES code was reduced to a one-dimensional column model, and the turbulence closure schemes described in Section 2 were used. The CBL depth was determined in the same manner as in LES, and the CBL depth versus time determinations were compared with those of LES.

The evaluation of the various schemes within the integral budget approach was done by retrieving the parameters B_s , z_i , Δb , Δu , and Δv from LES data and using them in the respective formulations (13), (14), or (15) with the constants indicated in Table 1. Unfortunately, the evaluation of the above parameters was not very straightforward. The definitions of the parameters of entrainment were dependent on the author evaluating them, regardless of whether the evaluation was made based on atmospheric data or LES results. For example, in the ZOM, the buoyancy jump across the entrainment zone can be evaluated in the strict sense of the ZOM, in which case the linear free atmospheric profile of buoyancy is extrapolated downward from the upper edge of the entrainment zone to the defined CBL depth z_i . However, many authors took the full change across the entire depth of the entrainment zone. Unfortunately, in most cases, the actual value of the parameterized heat flux at the inversion is highly sensitive to the size of the jumps used. Additionally, there is usually a difference between the actual entrainment heat flux, B_i (the minimum of heat flux in the entrainment zone), and the ZOM-parameterized heat flux, $\Delta b dz_i / dt$. Some authors have tuned their parameterizations for the former, and others for the latter. To the extent possible, this study tries to use the parameterizations in a manner consistent with the way they were originally evaluated by their respective authors.

Because of the large number of comparisons performed, only the most important and representative results are shown in the following sections.

5. RESULTS

5.1 RANS-Based Closures in NWP

The cases with a heat flux of 0.03 K/s and a free atmospheric stratification of 0.003 K/m are representative of the differences between the various numerical models of entrainment and LES. With this particular combination of surface heat flux and free atmospheric stratification, the shear promotes a significant deepening of the CBL in the GS and GC cases, relative to the shear-free (NS) case. The CBL depth versus time for the ARPS $e-l$ closure is compared with LES in Fig. 3. The CBL depth for the NS case grows more slowly with the ARPS $e-l$ model than with

LES. For the GC case, and particularly in the GS case, the relationship is reversed, and the $e-l$ model predicts faster CBL growth than is seen in LES.

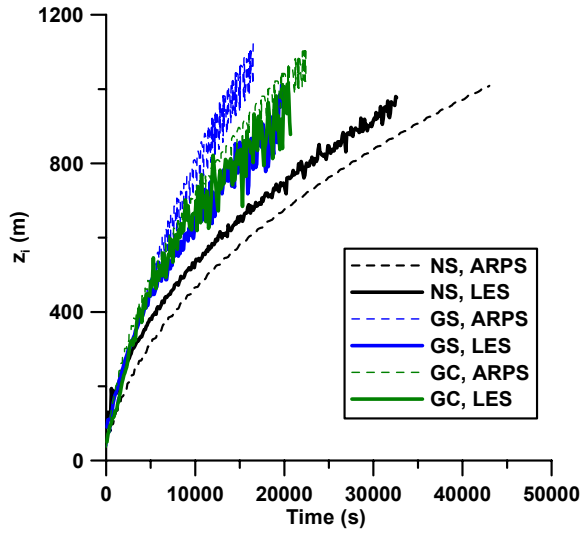


Figure 3. Comparison of the CBL depth (z_i) versus time predictions of ARPS $e-l$ closure versus LES

Figure 4 shows the heat flux profiles in LES versus the ARPS $e-l$ closure. In the LES, the heat flux profiles are generally smoother than in the ARPS closure, and it is obvious that, in the cases with shear, the RANS-based entrainment heat flux is much larger than in LES. Figure 5 shows the overall effect on the potential temperature profiles. If a different definition of the CBL depth, such as the height of the maximum temperature gradient, were used, the results would still be the same.

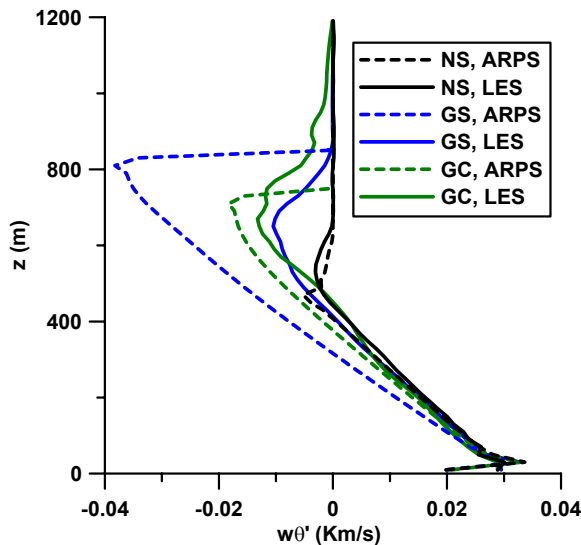


Figure 4. Comparison of the heat flux profiles of ARPS $e-l$ closure versus LES at $t=10000s$.

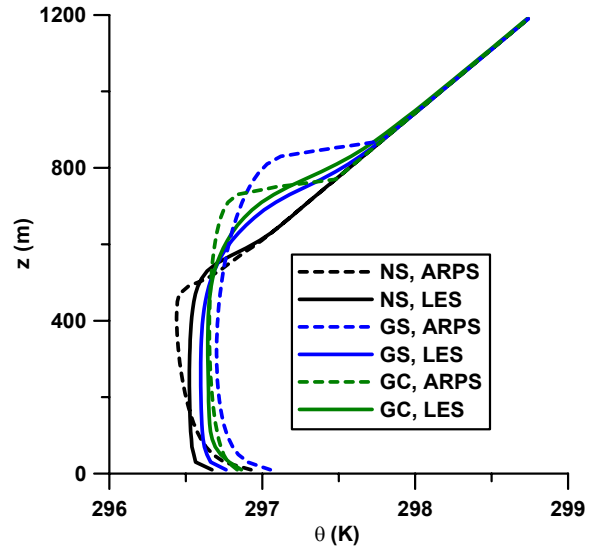


Figure 5. Comparison of the potential temperature profiles of ARPS $e-l$ closure versus LES at $t=10000s$.

The RANS-based closures predict much faster CBL growth compared to LES when shear is present. Figure 6 shows the TKE profiles. Surprisingly, the TKE in the ARPS $e-l$ closure is less than in LES, despite the greater entrainment of heat. Looking at the profile for the GS case more carefully, it can be seen that the TKE at the top of the CBL is greater in the ARPS $e-l$ closure than in LES. For the GC case, the LES has greater energy, but the energy calculations in LES do not distinguish between truly turbulent motions associated with entrainment and wave-like motions that do not mix heat.

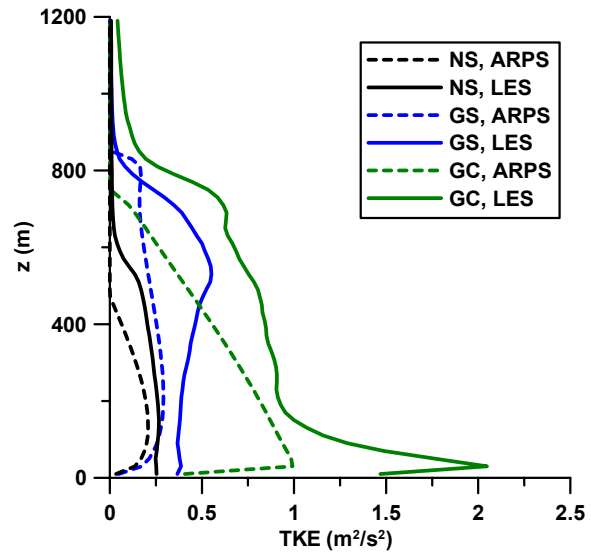


Figure 6. Comparison of the TKE profiles of ARPS $e-l$ closure versus LES at $t=10000s$.

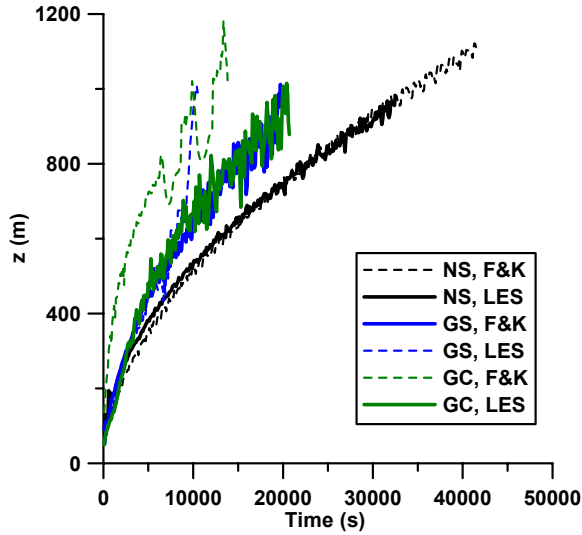


Figure 7. Comparison of the CBL depth z_i predictions with F&K $e-l$ closure and LES.

The F&K closure predictions of the CBL depth are compared with LES data in Fig. 7. Basically, the results, in a relative sense, are similar to those in the ARPS case. The CBL depths agree very closely with LES for the NS case, but in the GS and GC cases, the entrainment is remarkably faster than in LES.

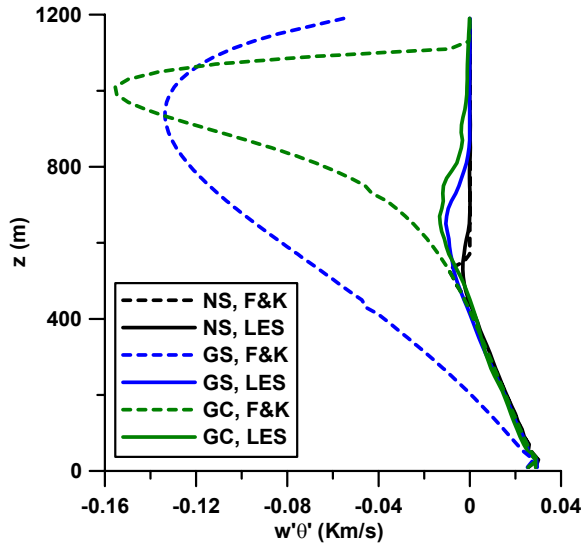


Figure 8. Comparison of the heat flux profiles obtained with F&K $e-l$ closure and LES at $t=10000s$.

The heat flux profiles are shown in Fig. 8. If the maximum temperature gradient height is used for the definition of the CBL depth, the results are very similar, as can be seen in Fig. 9. In Fig. 10, the TKE is shown. Unlike the ARPS closure, the F&K closure shows greater TKE in the cases with shear when compared to LES, and the TKE in the NS case is very comparable to

TKE from the LES. The TKE values in the interior of the CBL are actually rather similar to the LES predictions, but at the top of the CBL (where shear is fairly large), there is much more TKE predicted by F&K than by LES.

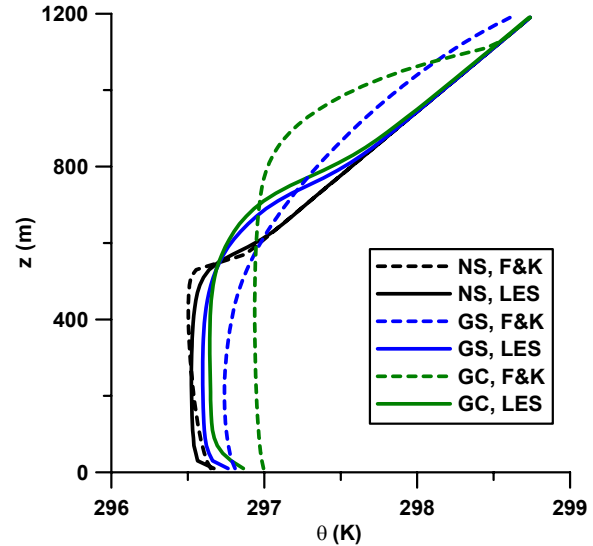


Figure 9. The potential temperature profiles from F&K $e-l$ and LES at $t=10000s$.

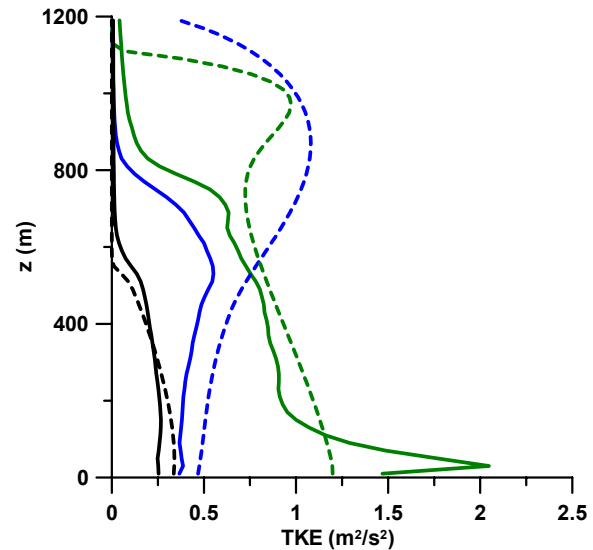


Figure 10. The TKE profiles from F&K $e-l$ and LES at $t=10000s$.

Finally, the momentum profiles in ARPS, F&K, and LES are compared in Fig. 11. Between the two $e-l$ models, the momentum gradients from F&K more closely match the LES momentum gradients than do those from ARPS, but the values of momentum are greater in the F&K data for the GS case because of the enhanced entrainment of momentum. The GC momentum from F&K is less than predicted by LES momentum for the CBL interior, perhaps due to the enhanced upward

mixing of weaker momentum from the surface. In ARPS, the TKE is much smaller in the lowest model grid level because of the greater dissipation there. This causes less frictional slowing of the momentum, and momentum throughout most of the CBL in ARPS is greater than the LES momentum for the GC case.

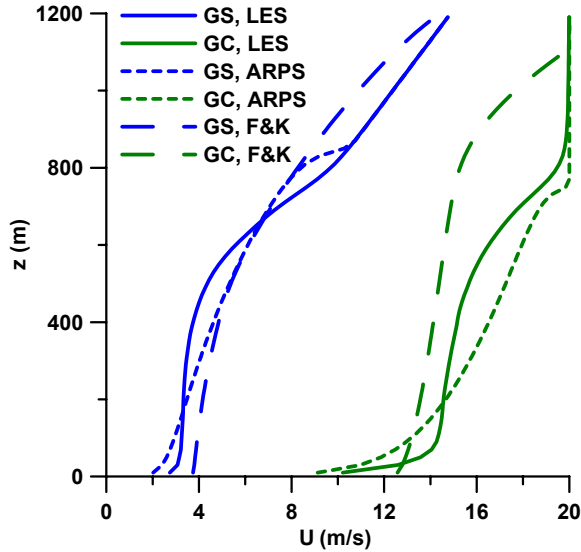


Figure 11. The momentum profiles from F&K $e-l$, ARPS, and LES at $t=10000s$.

The primary conclusion regarding performance of two considered $e-l$ closures is that for cases with shear, they predict faster entrainment than LES does. This overestimation is not as large with ARPS as it is with F&K, but the ARPS-predicted CBL growth in the NS case is also slower than in LES. Another common feature of the two closures is the larger relative difference in CBL entrainment between shear-free and sheared CBL cases than is predicted by LES. One more disadvantage of $e-l$ closures, earlier noted in Moeng and Wyngaard (1989), is their inability to directly account for counter-gradient turbulent flux in the upper portion of the CBL.

5.2 Integral Budget-Based Closure

The results of the integral budget methods are grouped according to the type of method. The parameterizations of Tennekes (1973), Driedonks (1982), and Batchvarova and Gryning (1990, 1994) take into account only the surface shear through their friction velocity terms and are presented together as Group I. The parameterizations of Zeman and Tennekes (1977), Tennekes and Driedonks (1981), Boers et al. (1984), and Pino et al. (2003) take into account more than just the surface shear. They also include either the spin-up term, velocity jump across the entrainment zone (although some may use the full jumps rather than the ZOM jumps), or both and are thus assigned to Group II. Finally, the parameterizations of Stull (1976a,b) and

Sorbjan (2004), which differ somewhat from the typical ZOM methodology, constitute Group III.

Figure 12 shows results obtained with the parameterizations of Group I for the GS case. The parameters of entrainment were retrieved from LES data. The black dots denote the entrainment flux ratio defined from the ZOM parameterization for the entrainment zone heat flux, $B_i = -\Delta b dz_i / dt$, and the blue dots denote the entrainment flux ratio defined from the actual minimum of buoyancy flux in the LES entrainment zone. Since the parameterizations in Fig. 12 take into account only the surface shear, which is initially zero, they underestimate the entrainment flux ratio in the GS case and predict values consistent with commonly accepted shear-free value of about 0.2.

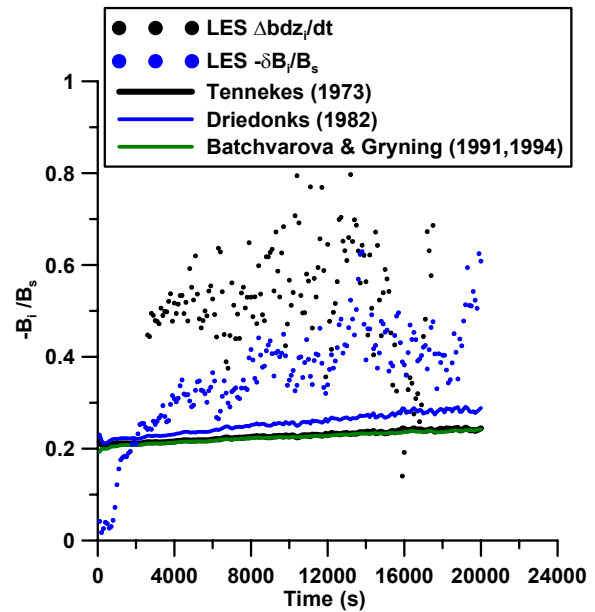


Figure 12. Entrainment flux ratio predictions of Group I closures compared with LES for the GS case with $d\theta/dz = 0.003 \text{ K/m}$ and $Q_s = 0.03 \text{ K m/s}$.

Figure 13 shows results for parameterizations from Group II. The entrainment parameterization of Zeman and Tennekes (1977) does not take entrainment zone shear into account and fortuitously performs better than the others when compared to LES data. Among those that do take the entrainment zone shear into account, the parameterization of Pino et al. (2003) performs the best, but all suffer from problems with the denominator going to zero, when the entrainment rate becomes unbounded.

Figure 14 shows the comparisons with the Group III parameterizations. Since these parameterizations do not include negative-sign shear terms in the denominator, the parameterized entrainment flux ratio does not become unbounded. The Stull (1976a,b) parameterization predicts an entrainment flux ratio that climbs steadily with time, while LES data show a fairly

constant value. The Sorbjan (2004) entrainment flux ratio also increases with time.

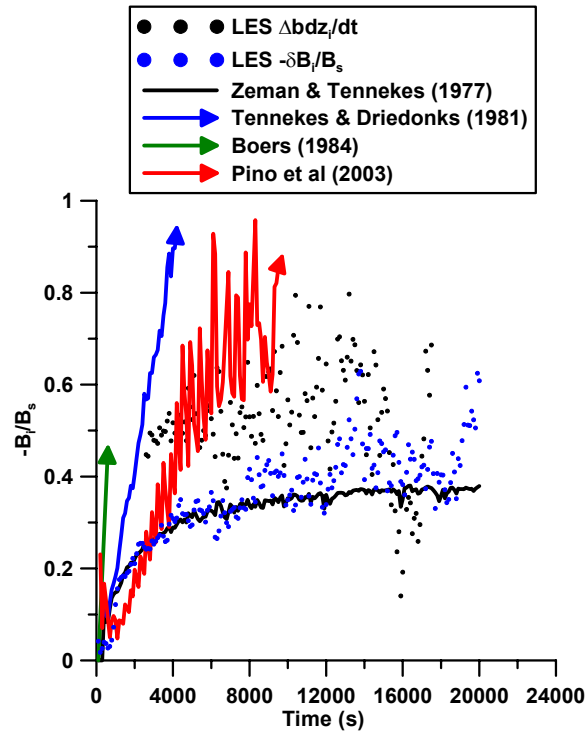


Figure 13. Entrainment flux ratio predictions by Group II closures compared to LES for the GS case with $d\theta/dz = 0.003$ K/m and $Q_s = 0.03$ K m/s.

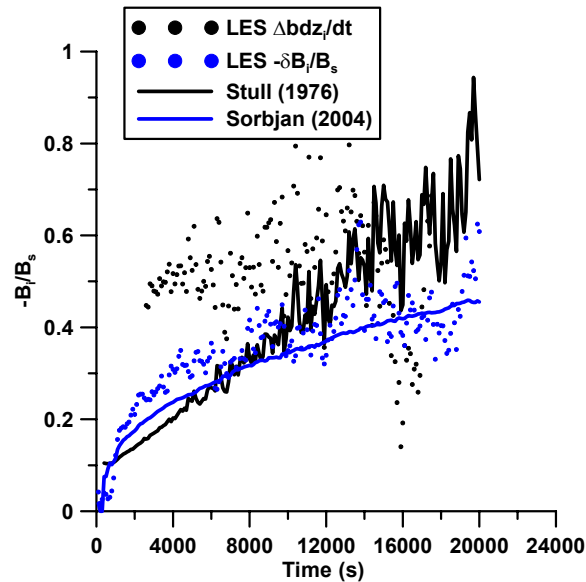


Figure 14. Entrainment flux ratio predictions by Group III closures compared to LES for the GS case with $d\theta/dz = 0.003$ K/m and $Q_s = 0.03$ K m/s.

Figure 15 shows the entrainment flux ratios by the Group I parameterizations for the GC case. All methods predict higher entrainment flux ratios than LES. The predicted ratios decrease with time, and the LES data show this decrease to some extent as well.

The initial value of surface shear is very large, and so the shear-generated TKE at the surface should be very large as well. As friction decreases the momentum in the CBL, the surface shear-generated TKE also decreases, resulting in a decrease in the predicted entrainment flux ratio.

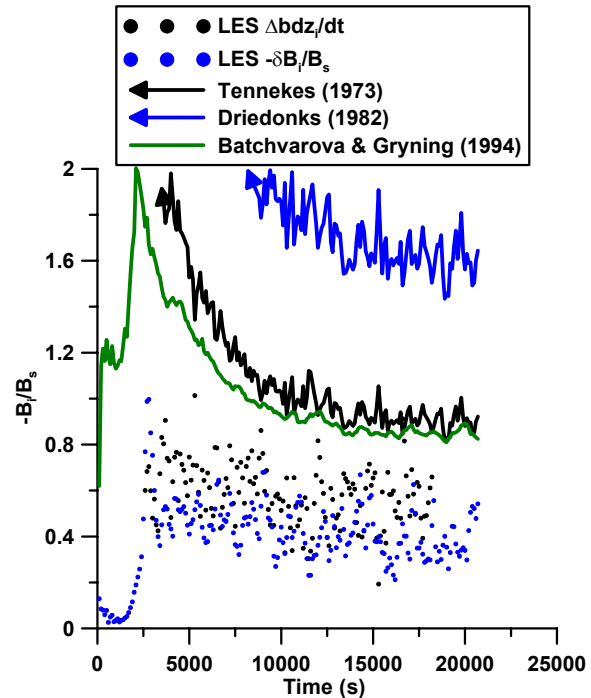


Figure 15. Entrainment flux ratio predictions of Group I closures compared to LES for the GC case with $d\theta/dz = 0.003$ K/m and $Q_s = 0.03$ K m/s.

Figure 16 shows entrainment predictions for the GC case by the Group II parameterizations. Again, all of them overpredict the entrainment flux ratio, but the Pino (2003) parameterization performs the best. The denominator goes to zero in these expressions for the GC case just like it does for the GS case.

Figure 17 shows performance of the Group III parameterizations for the GC case. These perform the best of all the groups of parameterizations. The parameterization of Stull (1976a,b), which takes both surface and elevated shears into account, performs better than the Sorbjan (2004) parameterization, which only uses entrainment zone shear. This does not necessarily mean that the surface shear is equally important to the entrainment zone shear. It merely means that the Stull parameterization is better tuned for this particular case. In fact, LES results indicate that it is primarily the entrainment zone shear that drives the enhancement of entrainment relative to the shear-free cases. Even the GC cases, which start without

entrainment zone shear, eventually develop similar shear at the CBL top when compared to the GS cases.

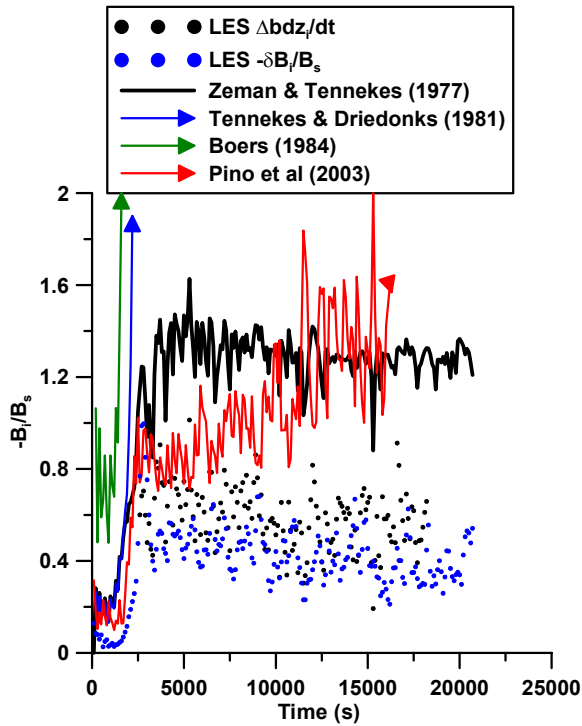


Figure 16. Entrainment flux ratio predictions of Group II closures compared to LES for the GC case with $d\theta/dz=0.003$ K/m and surface heat flux of 0.03 K m/s.

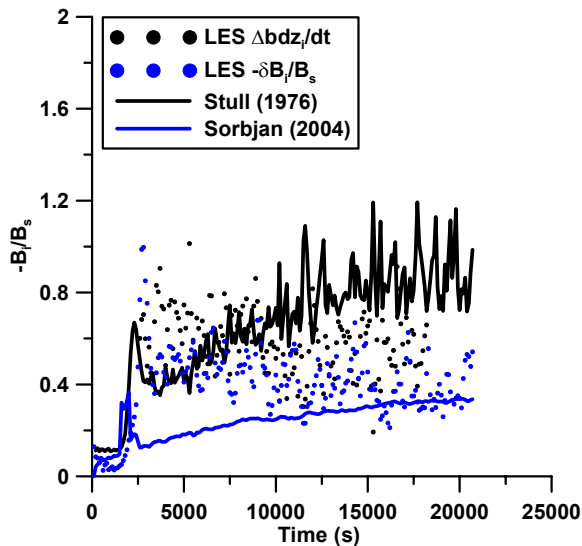


Figure 17. Entrainment flux ratio predictions of Group III closures compared to LES for the GC case with $d\theta/dz=0.003$ K/m and surface heat flux of 0.03 K m/s.

In order to illustrate a situation, in which the parameterizations perform reasonably well, we show in Fig. 18 the Group II parameterizations for the GS case

with a surface kinematic heat flux of 0.10 K m/s and a free atmospheric stratification of 0.010 K/m.

All parameterizations perform reasonably well, but the entrainment flux ratio is close to the shear-free value of 0.2 anyway. Of those methods that take entrainment zone shear into account, the Pino et al. (2003) parameterization is closest to the LES entrainment flux ratio. Overall, the Zeman and Tennekes (1977) parameterization is the closest to the LES results, but it does not specifically take the entrainment zone shear into account.

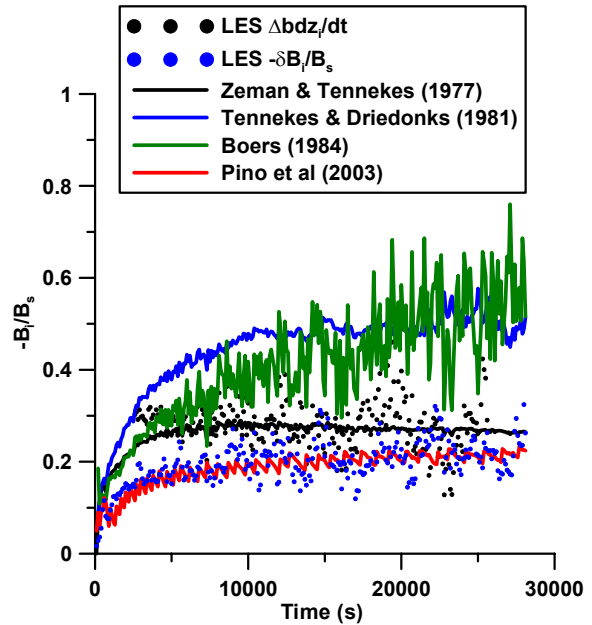


Figure 18. Entrainment flux ratio predictions by the Group II parameterizations compared to LES for the GS case with $d\theta/dz=0.010$ K/m and surface heat flux of 0.10 K m/s.

5. SUMMARY AND CONCLUSIONS

The $e-l$ closures of Xue et al. (2001) and Fielder and Kong (2003) both predict a greater difference in entrainment between shear-free CBLs and sheared CBLs, with entrainment predicted for sheared CBLs being too large. At the same time, the F&K closure predicts CBL growth very close to the LES predictions for the NS case. The more rapid entrainment in cases with shear seems to occur regardless of the TKE values in the parameterized CBL. The ARPS scheme produces less TKE than LES but still predicts too fast entrainment when shear is present. The F&K scheme generally produces TKE values that are comparable to those of LES, but the TKE in the entrainment zone, where significant shear is present, is significantly greater than the LES-predicted TKE. It is possible that the shear production of TKE in such schemes is overestimated, perhaps because the appropriate length scales for shear-generated turbulence in the CBL are different from the length scales for buoyancy-generated turbulence. It is possible that the formulation of the

master length scale l for CBL turbulence needs to be revised to account for the effects of shear.

The analysis in the present paper is somewhat limited by the fact that the initial momentum profiles do not necessarily reflect real atmospheric profiles. In particular, the surface winds in the GC case would probably never be equal to their geostrophic value, and so any NWP model initialization would have subgeostrophic winds at the surface and therefore weaker wind shears there. Likewise, the GS case has very large geostrophic shear, probably three or four times greater than its typical atmospheric value. Nevertheless, similar magnitudes of total shear (between 10 meters above ground level and a kilometer or so above ground level) are not unheard of. In this way, the cases with strong shear serve as a critical test of how an $e-l$ scheme in NWP might perform with respect to the development of the CBL. It is particularly important for NWP and air quality model schemes to correctly predict boundary layer depth, because this affects the concentration of moisture in the lower atmosphere as well as the concentration of air pollutants.

The tests of the integral budget-based entrainment schemes suggest that they overestimate entrainment in situations when strong shear is present. Again, it must be stated that the shear in the LES cases is rather strong, but the cases were designed in this manner so that the relative effects of shear could be more easily seen. Adhering to the strict mathematical form of the ZOM provides entrainment equations that contain the entrainment zone shear as a negative sign term in the denominator. This has the unfortunate result of causing the denominator to drop to zero and the entrainment heat ratio to become unbounded well before the surface heat flux goes to zero. Entrainment equations by Stull (1976a,b) and Sorbjan (2004), which deviate from the traditional ZOM methodology in this respect, avoid this problem and therefore produce more realistic results for the strong shear conditions. The success of these two parameterizations suggests the importance of accounting for the finiteness of the entrainment zone thickness in any entrainment equation for sheared CBL. Given that Kelvin-Helmholtz instabilities appear to be an inherent feature of convective entrainment in the presence of wind shears, as our and other LES show (see, e.g., Kim et al. 2003), any Ri -limited entrainment equation would seem to be most suited to model the growth dynamics of sheared CBL.

Acknowledgement: Authors gratefully acknowledge support by the National Science Foundation (grant ATM-0124068).

Ayotte, K. W., P. P. Sullivan, A. Andren, Scott C. Doney, A. A. M. Holtslag, W. G. Large, J. C. McWilliams, C.-H. Moeng, M. J. Otte, J. J. Tribbia, and J. C. Wyngaard, 1996: An evaluation of neutral and convective planetary boundary-layer parameterizations relative to large eddy simulations. *Bound. Layer Meteorol.*, **79**, 131-175.

- Batchvarova, E., and S.-E. Gryning, 1990: Applied model for the growth of the daytime mixed layer. *Bound.-Layer Meteor.*, **56**, 261-274.
- , and —, 1994: An applied model for the height of the daytime mixed layer and the entrainment zone. *Bound.-Layer Meteor.*, **71**, 311-323.
- Betts, A. K., 1974: Reply to comment on the paper "Non-precipitating Cumulus Convection and its Parameterization". *Quart. J. Roy. Meteorol. Soc.*, **100**, 469-471.
- Deardorff, J. W., 1970: Convective velocity and temperature scales for the unstable planetary boundary layer and for Raleigh convection. *J. Atmos. Sci.*, **27**, 1211-1213.
- Driedonks, A. G. M., 1982: Models and observations of the growth of the atmospheric boundary layer. *Bound.-Layer Meteor.*, **23**, 283-306.
- Fairall, C. W., 1984: Wind shear enhancement of entrainment and refractive index structure parameter at the top of a turbulent mixed layer. *J. Atmos. Sci.*, **41**, 3472-3484.
- Fedorovich, E., 1995: Modeling the atmospheric convective boundary layer within a zero-order jump approach: an extended theoretical framework. *J. Appl. Meteor.*, **34**, 1916-1928.
- , R. Conzemius, and D. Mironov, 2004: Convective entrainment into a shear-free linearly stratified atmosphere: bulk models reevaluated through large eddy simulations. *J. Atmos. Sci.*, **61**, 281-295.
- Fiedler, B. H., and F. Kong, 2003: The performance of an $E-l$ scheme for the atmospheric boundary layer in a mesoscale model with grid spacing as small as 1 km. *Meteorol. Atmos. Phys.*, **84**, 1-10.
- Kim, S.-W., 2001: Entrainment parameterization in sheared convective boundary layers. Ph.D. Thesis, Korean National University, Seoul.
- , Park, S.-U., and Moeng, C.-H., 2003: Entrainment processes in the convective boundary layer with varying wind shear. *Bound.-Layer Meteor.*, **108**, 221-245.
- Lilly, D. K., 1968: Models of cloud-topped mixed layers under a strong inversion. *Quart. J. Roy. Meteor. Soc.*, **94**, 292-309.
- Mahrt, L., and D. H. Lenschow, 1976: Growth dynamics of the convectively mixed layer. *J. Atmos. Sci.*, **33**, 41-51.
- Moeng, C.-H. and J. C. Wyngaard, 1989: Evaluation of turbulent transport and dissipation closures in second-order modeling. *J. Atmos. Sci.*, **46**, 2311-2330.
- Pino, D., J. V.-G. de Arellano, and P. J. Duynkerke, 2003: The contribution of shear to the evolution of a convective boundary layer. *J. Atmos. Sci.*, **60**, 1913-1926.
- Sorbjan, Z., 2004: Large-eddy simulations of the baroclinic mixed layer. *Bound.-Layer Meteor.*, **112**, 57-80.
- Stull, R. B., 1976a: The energetics of entrainment across a density interface. *J. Atmos. Sci.*, **33**, 1260-1267.
- , 1976b: Mixed-layer depth model based on turbulent energetics. *J. Atmos. Sci.*, **33**, 1268-1278.

- Tennekes, H., 1973: A model for the dynamics of the inversion above a convective boundary layer. *J. Atmos. Sci.*, **42**, 558-567.
- , and A. G. M. Driedonks, 1981: Basic entrainment equations for the atmospheric boundary layer. *Bound.-Layer Meteor.*, **20**, 515-531
- Xue, M., K. K. Droegemeier, and V. Wong, 2000: The advanced regional prediction system (ARPS) – a multi-scale nonhydrostatic atmospheric simulation and prediction model. Part I: Model dynamics and verification. *Meteorol. Atmos. Phys.*, **75**, 161-193.
- Zeman, O., and H. Tennekes, 1977: Parameterization of the turbulent energy budget at the top of the daytime atmospheric boundary layer. *J. Atmos. Sci.*, **34**, 111-123.
- Zilitinkevich, S. S., and J. W. Deardorff, 1974: Similarity theory for the planetary boundary layer of time-dependent height. *J. Atmos. Sci.*, **31**, 1449–1452.